Keynote Paper
Delivered at the Eighth International Heat Transfer Conference
San Francisco, CA August 17-22, 1986

RECENT DEVELOPMENTS IN THERMAL CONTACT, GAP AND JOINT CONDUCTANCE THEORIES AND EXPERIMENT

M. Michael Yovanovich

Department of Mechanical Engineering, University of Waterloo
Waterloo, Ontario, Canada

Thermal contact, gap and joint conductance models developed for point and line contacts as well as conforming rough surfaces are reviewed and up-dated. The theory is compared with recently obtained experimental values. The agreement between the model predictions and the experimental results are very good to excellent for the point contacts and the conforming rough models. The significant discrepancies observed at light loads in the line contacts are attributed to errors in form (crowning). The differences in the conforming rough model at light loads are due to several factors; the major one being high local strains due to very large local temperature gradients.

1. INTRODUCTION

Steady-state heat transfer across interfaces formed by two contacting solid bodies is usually accompanied by measurable temperature drops across the joint because there is thermal resistance to heat flow within the region of the interface. The temperature drop (ΔT_c) at the interface is obtained by extrapolation of the steady-state one-dimensional temperature distribution from regions "far" from the interface.

The contact conductance or contact coefficient of heat transfer is defined as:

$$h = (Q/A_a)/\Delta T_c \qquad (1)$$

where (Q/A_a) is the steady-state heat flux based upon the apparent contact area. The thermal contact resistance is defined as the temperature drop at the interface divided by the total heat flow rate. Thus

$$R = \Delta T_c/Q \qquad (2)$$

and, therefore, we can write the following relationship between the thermal contact resistance and the contact conductance:

$$R = 1/h\ A_a \qquad (3)$$

The thermal resistance concept will be used throughout this paper because this concept lends itself to mathematical analysis. Whenever reference is made to thermal conductance, the reciprocal of the product of the thermal resistance and apparent contact area is implied. Real surfaces are not perfectly smooth (specially prepared surfaces such as those found in bearings can be considered to be almost ideal surfaces) but consist of microscopic peaks and valleys. Whenever two real surfaces are placed in contact, intimate solid to solid contact occurs only at discrete parts of the interface and the real contact area will represent a very small fraction (<5%) of the nominal contact area.

The real interface is characterized by several important factors:

1) Intimate contact occurs at discrete parts of the nominal interface.

2) The ratio of the real contact area to the nominal contact area is usually much less than 5%.

3) The pressure at the real contact is much greater than the apparent contact pressure. The real contact pressure is related to the flow pressure of the contacting peaks.

4) A very thin gap exists in the regions in which there is no intimate contact, and it is usually occupied by a third substance.

5) The third substance can be air, other gases, liquid, grease or another metal.

6) The interface is idealized as a line but the actual thickness of the interface ranges from 0.5 μm for smooth surfaces to about 60 μm for very rough surfaces.

7) Heat transfer across the interface can take place by conduction through the real contact area, by conduction through the substance in the gap or by radiation across the gap if in vacuum. It is possible that all three modes of heat transfer occur simultaneously, but usually they occur in pairs.

The process of heat transfer across an interface is complex because the thermal resistance can depend upon many parameters of which the following are very important:

a) geometry of the contacting solids: surface roughness and waviness
b) thickness of the gap (non-contact region)
c) type of interstitial fluid: gas, liquid, grease, vacuum
d) interstitial gas pressure
e) thermal conductivities of the contacting solids and the interstitial substance
f) hardness or flow pressure of the contacting asperities: plastic deformation of the highest peaks

g) modulus of elasticity of the contacting solids: elastic deformation of the wavy parts of the interface
h) average temperature of the interface: radiation effects as well as property effects

Because thermal contact resistance is such a complex problem, it is necessary to develop simple thermophysical models which can be analysed and experimentally verified. To achieve these goals the following assumptions have been made in the development of the several contact resistance models:

a) contacting solids are isotropic: thermal conductivity and physical parameters are constant
b) contacting solids are thick relative to the roughness or the waviness
c) surfaces are clean: no oxide effect
d) contact is static: no vibration effects
e) first loading cycle only: no hysteresis effects
f) apparent contact pressure is not too small nor too large
g) radiation is very small or negligible
h) heat flux is steady and not too large
i) contact is made in a vacuum or the interstitial fluid can be considered to be a continuum if it is not a gas.
j) the interstitial fluid perfectly wets both contacting solids

2. ELASTOCONSTRICTION AND GAP RESISTANCES

The elastoconstriction and elastogap resistance models are based upon the Boussinesq point load model and the Hertz distributed load model. Both models assume the bodies have smooth surfaces, they are perfectly elastic, and the applied load is static and normal to the plane of the contact area. In the general case the contact area will be elliptical having semimajor and semiminor axes a,b respectively. These dimensions are much smaller than the dimensions of the contacting bodies. The thermal resistance model is based upon the assumption that both contacting bodies can be modelled as half-spaces. The circular contact area produced when two spheres or a sphere and a flat are in contact are two special cases of the elliptical contact. Also the rectangular contact area produced when two ideal circular cylinders are in line contact or an ideal cylinder and a flat are in contact are also special cases of the elliptical contact area [1,2].

2.1 The Hertz Contact Parameters

Contact area shape and size. Whenever a solid, denoted as body 1, is brought into contact with another solid, denoted as body 2, the Hertzian theory predicts an elliptical contact whose semiaxes are related to the mechanical load, physical properties and geometry as follows [3-7]:

$$a = m\left[\frac{3\,N\,\Delta}{2(A+B)}\right]^{1/3} \tag{4}$$

and

$$b = n\left[\frac{3\,N\,\Delta}{2(A+B)}\right]^{1/3} \tag{5}$$

In Eqs. (4) and (5), N is the total normal load acting upon the contact area, and Δ is a physical parameter defined as

$$\Delta = [(1-\nu_1^2)/E_1 + (1-\nu_2^2)/E_2]/2 \tag{6}$$

when dissimilar materials form the contact. The physical parameters appearing in Eq. (6) are Young's modulus, E_1 and E_2, and Poisson's ratio ν_1 and ν_2.

The geometric parameter in Eqs. (4) and (5) is

$$2(A+B) = \frac{1}{\rho_1} + \frac{1}{\rho_1'} + \frac{1}{\rho_2} + \frac{1}{\rho_2'} = \frac{1}{\rho^*} \tag{7}$$

and the local radii of curvature of the contacting solids are denoted as ρ_1, ρ_1', ρ_2 and ρ_2'.

An additional relationship between A and B required in the Hertzian theory is

$$2(B-A) = \left[\left(\frac{1}{\rho_1} - \frac{1}{\rho_1'}\right)^2 + \left(\frac{1}{\rho_2} - \frac{1}{\rho_2'}\right)^2 + 2\left(\frac{1}{\rho_1} - \frac{1}{\rho_1'}\right)\left(\frac{1}{\rho_2} - \frac{1}{\rho_2'}\right)\cos 2\phi\right]^{1/2} \tag{8}$$

The parameter ϕ is the angle between the principal planes which pass through the contacting solids.

The dimensionless parameters m and n which appear in Eqs. (4) and (5) are called the Hertz elastic parameters. They are determined by means of the following Hertz relationships [3-7]:

$$m = [(2/\pi)E(k')/k^2]^{1/3} \tag{9}$$

and

$$n = [(2/\pi)kE(k')]^{1/3} \tag{10}$$

where E(k') is the complete elliptic integral of the second kind of modulus k', and

$$k' = (1 - k^2)^{1/2} \tag{11}$$

and $k = \frac{n}{m} = \frac{b}{a} \leq 1$.

The additional parameters k and k' are solutions of the transcendental equation [3-7]:

$$\frac{B}{A} = \frac{(1/k^2)E(k') - K(k')}{K(k') - E(k')} \tag{12}$$

where K(k') and E(k') are complete elliptic integrals of the first and second kind of modulus k'[8].

The Hertz solution requires the calculation of k, the ellipticity, K(k') and E(k'). This calls for the solution of Eq. (12) which relates k, K(k') and E(k') to the local geometry of the contacting solids. This is usually done by some iterative numerical procedure [5,6] or with the aid of tables [4].

To this end, additional parameters have been defined:

$$\cos\tau = (B-A)/(B+A) \tag{13}$$

and

$$\omega = A/B \leq 1 \tag{14}$$

and computed values of m and n, or (m/n) and n, are presented with τ or ω as the independent parameter. Table 1 shows how k, m and n depend upon the parameter ω over a range of values which should cover most contact problems.

Blahey [22] has shown that k' which is the solution of Eq. (12) can be computed accurately and efficiently by means of the Newton-Raphson iteration method applied to the following expression:

Table 1 Hertz Contact Parameters and Elastoconstriction Parameter

ω	k	m	n	ψ^*
0.001	0.0147	14.316	0.2109	0.2492
0.002	0.0218	11.036	0.2403	0.3008
0.004	0.0323	8.483	0.2743	0.3616
0.006	0.0408	7.262	0.2966	0.4020
0.008	0.0483	6.499	0.3137	0.4329
0.010	0.0550	5.961	0.3277	0.4581
0.020	0.0828	4.544	0.3765	0.5438
0.040	0.1259	3.452	0.4345	0.6397
0.060	0.1615	2.935	0.4740	0.6994
0.080	0.1932	2.615	0.5051	0.7426
0.100	0.2223	2.391	0.5313	0.7761
0.200	0.3460	1.813	0.6273	0.8757
0.300	0.4504	1.547	0.6969	0.9261
0.400	0.5441	1.386	0.7544	0.9557
0.500	0.6306	1.276	0.8045	0.9741
0.600	0.7117	1.1939	0.8497	0.9857
0.700	0.7885	1.1301	0.8911	0.9930
0.800	0.8618	1.0787	0.9296	0.9972
0.900	0.9322	1.0361	0.9658	0.9994
1.000	1.0000	1.0000	1.0000	1.0000

$$k'_{new} = k' + \frac{N(k')}{D(k')} \tag{15}$$

where

$$N(k') = k^2 \frac{E(k')}{K(k')} \left[k^2 + \frac{A}{B}\right] - k^4\left[1 + \frac{A}{B}\right] \tag{16}$$

and

$$D(k') = \frac{E(k')}{K(k')} \left[k'k^2 - 2k'\left(\frac{A}{B}\right)\right] + \left(\frac{A}{B}\right) k^2k' \tag{17}$$

If the initial guess for k' is based upon the following correlation of the results given in Table 1, the convergence will occur within 2 to 3 iterations:

$$k' = \left\{1 - \left[0.9446\left(\frac{A}{B}\right)^{0.6135}\right]^2\right\}^{1/2} \tag{18}$$

Polynomial approximations [8] of the complete elliptic integrals appearing in Eqs. (15-17) can be used to evaluate them with an absolute error less than 10^{-7} over the full range of k'.

Local gap thickness. The local gap thickness is required for the development of the elastogap resistance model.

The general expression for the gap thickness can be determined by means of geometric arguments:

$$\delta(x,y) = \delta_o(x,y) + w(x,y) - w_o \tag{19}$$

where $\delta_o(x,y)$ is the local gap thickness under zero load conditions, $w(x,y)$ is the total local displacement of the surfaces of the bodies outside the loaded area, and w_o is the approach of the contact bodies due to loading.

The total local displacement of the two bodies is given by

$$w(x,y) = \frac{3N\Delta}{2\pi} \int_{\mu}^{\infty} \left(1 - \frac{x^2}{a^2+t} - \frac{y^2}{b^2+t}\right) \frac{dt}{\{(a^2+t)(b^2+t)t\}^{1/2}} \tag{20}$$

where μ is the positive root of the equation

$$x^2/(a^2+\mu) + y^2/(b^2+\mu) = 1 \tag{21}$$

When μ>0, the point of interest lies outside the elliptical contact area

$$x^2/a^2 + y^2/b^2 = 1 \tag{22}$$

When μ=0, the point of interest lies inside the contact area, and when x=y=0, $w(0,0)=w_o$ the total approach of the contacting bodies is:

$$w_o = \frac{3N\Delta}{2\pi} \int_{o}^{\infty} \frac{dt}{\{(a^2+t)(b^2+t)t\}^{1/2}} \tag{23a}$$

$$= \frac{3N\Delta}{\pi a} K(k') \tag{23b}$$

2.2.1 Sphere-Flat Hertz Contact Parameters

The previously developed Hertz contact parameters reduce to simple expressions for the case of a sphere ($\rho_1 = \rho'_1 = D/2$) in contact with a flat ($\rho_2 = \rho'_2 = \infty$). In this instance the parameters A and B are determined by (A+B) = 2/D and (B-A) = 0 to be B = A = 1/D. When B/A = 1, Eq. (12) gives k = 1 and Eqs. (9) and (10) give m = n = 1. The contact area is circular with radius a determined by means of the following dimensionless expression:

$$2a/D = [3N\Delta/D^2]^{1/3} \tag{24}$$

The local gap thickness is axisymmetric, and can be determined by the following dimensionless expression:

$$\frac{2\delta}{D} = 1 - (1 - x^2/L^2)^{1/2} + [(2-x^2)\sin^{-1}(1/x) + (x^2-1)^{1/2}]/\pi L^2 - 1/L^2 \tag{25}$$

where L = D/2a, x = r/a and $1 \le x \le L$.

2.2.2 Cylinder-Flat Hertz Contact Parameters

When an ideal circular cylinder ($\rho_1 = D/2, \rho'_1 = \infty$) is in elastic contact with a flat ($\rho_2 = \rho'_2 = \infty$), the contact width 2b of the rectangular area can be determined by the dimensionless expression:

$$2b/D = 4(N\Delta/\pi\ell D)^{1/2} \tag{26}$$

where ℓ is the cylinder length.

The local gap thickness is obtained from the following dimensionless expression [7]:

$$2\delta/D = (1 - 1/L^2)^{1/2} - (1 - \xi^2/L^2)^{1/2} + [\xi(\xi^2 - 1)^{1/2} - \cosh^{-1}(\xi) - \xi^2 + 1]/2L \tag{27}$$

where L = D/2b, ξ = x/L and $1 \le \xi \le L$.

3.1. Ellipsoidal Constriction Resistance

Yovanovich has developed a general constriction resistance model [1] which is based upon the assumption that each body forming an elliptical contact area can be taken to be a conducting half-space. This approximation of actual bodies is reasonable because the dimensions of the contact area are very small relative to the characteristic dimensions of the contact bodies.

When the free surfaces of the contacting bodies are adiabatic, the total ellipsoidal constriction resistance of an isothermal elliptical contact area (a > b) is [1]

$$R_e = \psi_e/2\, k_s a \tag{28}$$

where a is the semimajor axis, k_s is the harmonic mean thermal conductivity,

$$k_s = 2\, k_1k_2/(k_2 + k_2) \tag{29}$$

and ψ_e is the isothermal elliptical constriction parameter [3]:

$$\psi_e = (2/\pi)K(k') \tag{30}$$

in which K(k') is the complete elliptic integral of the first kind of modulus k', and it is related to the axes:

$$k' = [1 - (b/a)^2]^{1/2} \tag{31}$$

The complete elliptic integral can be computed accurately by means of Chebyshev polynomial approximations [8] or by means of the Arithmetic-Geometric-Mean (AGM)[8]. This important special function can also be approximated by means of the following simple expressions:

$$K(k') = \ell n(4a/b) \qquad 0 \leq k < .1736 \tag{32a}$$

$$K(k') = 2\pi/[1 + \sqrt{(b/a)}]^2 \qquad .1736 < k \leq 1 \tag{32b}$$

This approximation has a maximum error less than 0.8% and it occurs at k = 0.1736. The ellipsoidal constriction parameter reduces to the value of one when a = b, a circular contact area.

3.2.1. Elastoconstriction Resistance of Point Contacts

When the results of the Hertz elastic deformation analysis are substituted into the results of the Yovanovich ellipsoidal constriction analysis, one obtains the elastoconstriction resistance expression [3]:

$$k_s[24N\Delta\rho^*]^{1/3} \quad R_e = (2/\pi)[K(k')/m] \equiv \psi^* \tag{33}$$

where the effective radius of the ellipsoidal contact is defined as $\rho^* = [2(A+B)]^{-1}$. The left hand side of Eq. (33) is a dimensionless group consisting of the known total mechanical load N, the thermal conductivity k_s, the physical parameter Δ and the isothermal, elliptical constriction resistance R_e. The right hand side is defined to be ψ^* which is called the thermal elastoconstriction parameter [3]. Typical values of ψ^* for a range of values of ω are given in Table 1. The elastoconstriction parameter ψ^* reduces to unity when k = b/a = 1, the case of the circular contact area.

The elastoconstriction resistance of a sphere-flat contact can be derived from the ellipsoidal constriction resistance, Eq. (33), by putting $\psi^* = 1$, $\rho^* = D/4$ and employing the sphere diameter to nondimensionalize the result:

$$k_s D R_c = L \tag{34}$$

3.2.2. Elastoconstriction Resistance of Line Contacts

The thermal constriction resistance of a joint consisting of an ideal smooth circular cylinder in contact with a smooth flat was developed by McGee, Schankula and Yovanovich [12]. This model is based upon the constriction resistance of an isothermal strip contact, of width 2b, placed on the surface of a half-cylinder of diameter D, denoted as body 1. This model also uses the result for the constriction resistance of an isothermal strip, of width 2b, on a flat of width D, denoted as body 2 [9,10].

The constriction resistance of body 1 is

$$R_{c1} = (1/\ell\pi k_1)\ell n(2D/b) - 1/2\ell k_1 \tag{35}$$

and that of body 2,

$$R_{c2} = (1/\ell\pi k_2)\ell n(D/\pi b) \tag{36}$$

The total elastoconstriction resistance is the sum which when multiplied by k_s and ℓ becomes [12]

$$\ell k_s R_c = \frac{k_s}{k_1}\frac{1}{2\pi}\ell n(\pi/N^*) - \frac{k_s}{2k_1} - \frac{k_s}{k_2}\frac{1}{2\pi}\ell n(4\pi N^*) \tag{37}$$

where k_s is the harmonic mean thermal conductivity defined by Eq. (29) and N^* is the dimensionless mechanical load [12]:

$$N^* = N\Delta/\ell D \tag{38}$$

When $k_1 = k_2$, Eq. (37) reduces to the following expression:

$$\ell k_s R_c = (1/\pi)\ell n(1/N^*) - 0.7206 \tag{39}$$

3.3. Elastogap Resistance Model

The thermal resistance of the gas-filled gap depends upon three local quantities: the local gap thickness, the thermal conductivity of the gas, and the temperature difference between the solid bounding surfaces.

The gap model is based upon the subdivision of the gap into elemental heat flow channels (flux tubes) having isothermal upper and lower boundaries, and adiabatic sides. The heat flow lines in each channel are assumed to be straight and perpendicular to the plane of contact.

If the local gas conductivity, $k_g(x,y)$, in each elemental channel is assumed to be uniform across the local gap thickness $\delta(x,y)$, then the differential gap heat flow rate is

$$dQ_g = \frac{k_g(x,y)\Delta T_g(x,y)}{\delta(x,y)}\,dxdy \tag{40}$$

The total gap heat flow rate is given by the double integral

$$Q_g = \iint_{A_g} dQ_g \tag{41}$$

where the integration is performed over the entire effective gap area.

The thermal resistance of the gap, R_g, is defined in terms of the overall joint temperature drop, ΔT_c:

$$\frac{1}{R_g} = \frac{Q_g}{\Delta T_c} = \iint_{A_g}\frac{k_g(x,y)\Delta T_g(x,y)}{\delta(x,y)\Delta T_c}\,dxdy \tag{42}$$

The local gap thickness in the general case of two bodies in elastic contact forming an elliptical contact area is given by Eq. (19).

The local gas conductivity is based upon a model suggested by Kaganer [13] for the effective thermal conductivity of a gaseous layer bounded by two infinite, isothermal, parallel plates. Therefore for each heat flow channel the conductivity is

$$k_g(x,y) = k_{g,\infty}/[1 + \frac{\alpha\beta\Lambda}{\delta(x,y)}] \tag{43}$$

where $k_{g,\infty}$ is the gas conductivity under continuum conditions at STP. The accommodation parameter, α, is defined as

$$\alpha = (2-\alpha_1)/\alpha_1 + (2 - \alpha_2)/\alpha_2 \tag{44}$$

where α_1 and α_2 are the accommodation coefficients at the solid-gas interfaces. The fluid property parameter, β, is defined by

$$\beta = (2\gamma)/(\gamma+1)/Pr \tag{45}$$

where γ is the ratio of the specific heats, and Pr is the Prandtl number. The mean free path, Λ, of the gas molecules is given in terms of $\Lambda_{g,\infty}$, the mean free path at STP, as follows:

$$\Lambda = \Lambda_{g,\infty}(T_g/T_{g,\infty})(P_{g,\infty}/P_g) \quad (46)$$

Two models for determining the local temperature difference, $\Delta T_g(x,y)$, are proposed. In the first model it is assumed that the bounding solid surfaces are isothermal at their respective contact temperatures; hence

$$\Delta T_g(x,y) = \Delta T_c \quad (47)$$

This is called the thermally decoupled model, since it assumes that the surface temperature at the solid-gas interface is independent of the temperature field within each solid.

In the second model, it is assumed that the temperature distribution of the solid-gas interface is induced by the conduction through the solid-solid contact, under vacuum conditions [1]. This temperature distribution is approximated by the temperature distribution immediately below the surface of an insulated half-space that receives heat from an isothermal elliptical contact. Solving for this temperature distribution, using ellipsoidal coordinates, Yovanovich [1] found that

$$\Delta T_g(x,y)/\Delta T_c = 1 - F(k',\psi)/K(k') \quad (48)$$

where $F(k',\psi)$ is the incomplete elliptic integral of the first kind of modulus k' and amplitude angle ψ. The modulus, k', is defined Eq. (11) and the amplitude angle by

$$\psi = \sin^{-1}[a^2/(a^2+\mu)]^{1/2} \quad (49)$$

where the parameter μ is defined by Eq. (21). It ranges between $\mu = 0$, the edge of the elliptical contact area, to $\mu = \infty$, the distant points within the half-space.

Since the solid-gas interface temperature is coupled to the interior temperature distribution, Eq. (48) is called the coupled half-space model temperature drop.

The general elastogap model, Eq. (42), has not been solved. Two special cases of the general model have been considered by Yovanovich and co-workers [3,12,16,19].

Elastogap model for point contacts. This model was developed for the sphere-flat contact, and the gap resistance defined by Eq. (42) was found to be

$$1/R_g = (D/L)k_{g,\infty} I_p \quad (50)$$

The point contact gap integral, I_p, is defined as [19]

$$I_p(L,M) = \int_1^L \frac{2x\tan^{-1}(x^2-1)^{1/2}}{(2\delta/D) + M}\, dx \quad (51)$$

where the gas parameter, M, is defined to be

$$M = 2\alpha\beta\Lambda/D \quad (52)$$

The dimensionless local gap thickness is determined by Eq. (25).

The point contact gap resistance, Eq. (50), can be made dimensionless using k_s and D as was done in Eq. (34) for the constriction resistance. Thus Eq. (50) becomes

$$1/R_g^* = (\kappa/D)I_p \quad (53)$$

where $\kappa = k_{g,\infty}/k_s$, the thermal conductivity ratio.

Elastogap model for line contacts. This model was developed for the ideal cylinder-flat contact, and the gap resistance defined by Eq. (42) was found to be [12]

$$1/R_g = (4b\ell/D)k_{g,\infty} I_\ell \quad (54)$$

The line contact gap integral, I_ℓ, is defined as [12]

$$I_\ell(L,M) = \frac{2}{\pi}\int_1^L \frac{\cosh^{-1}(\xi)d\xi}{2\delta(\xi)/D + M} \quad (55)$$

The gas parameter M is defined in Eq. (52) and the dimensionless local gap thickness is given by Eq. (27).

The line contact gap resistance, Eq. (54), can also be made dimensionless by multiplying R_g by the $k_s D$ product to give

$$1/R_g^* = (4b\ell/D^2)\kappa I_\ell \quad (56)$$

3.4. Radiative Gap Resistance

The radiative resistance is a complex parameter depending upon the geometry of the gap, the emissivities of the contacting solids and the side walls forming the enclosure, as well as the temperature distribution of the bounding surfaces.

The radiative heat transfer rate across the gap formed by a hemisphere (or a portion of a larger hemisphere) and a circular disk of the same diameter enclosed by insulation has been modelled as a grey enclosure. The emissivities of the hemisphere, disk and sidwalls are denoted as ε_1, ε_2, and ε_3 respectively. Assuming isothermal hemisphere and flat at temperatures T_1 and T_2 respectively, the net radiative heat transfer rate is

$$Q_r = A_1\bar{f}_{21}\sigma[T_1^4 - T_2^4] \quad (57)$$

where the effective radiative heat transfer area is $A_1 = (\pi D^2/4)(1 - 1/L^2)$ and σ is the Stefan-Boltzmann constant. The grey-body view factor $\bar{f}_{12}$ for the enclosure is [16]:

$$\{\bar{f}_{21}\}^{-1} = (1 - \varepsilon_2/\varepsilon_3) + (A_2/A_1)(1 - \varepsilon_1)/\varepsilon_1 + \frac{1}{\bar{F}_{21} + \{1/\bar{F}_{23} + (A_2/A_1)/\bar{F}_{13}\}^{-1}} \quad (58)$$

When the view factors are evaluated and using the appropriate reciprocity relationship one obtains [16]:

$$\{\bar{f}_{21}\}^{-1} = (1 - \varepsilon_2)/\varepsilon_2 + (1 - \varepsilon_1)/(2\varepsilon_1) + 1.104 \quad (59)$$

For moderate temperature drops across the gap, the radiative resistance defined as $R_r = (T_1 - T_2)/Q_r$ can be approximated by

$$R_r = 1/A_2\bar{f}_{21}\, 4\sigma T_m^3 \quad (60)$$

where $T_m = (T_1 + T_2)/2$, the mean absolute temperature of the gap.

The dimensionless radiative resistance $R_r^* = k_s D R_r$ with $\bar{f}_{21}$ determined by means of Eq. (59) can now be expressed as

$$R_r^* = k_s\{(1 - \varepsilon_2)/\varepsilon_2 + (1 - \varepsilon_1)/(2\varepsilon_1) + 1.104\}/\pi D_2\sigma T_m^3 \quad (61)$$

3.5. Dimensionless Joint Resistance

The overall joint resistance will depend upon the solid-solid resistance called the constriction resistance, the gap resistance and the radiative resistance across the gap when a non-participating gas is present.

In the simplest model it is assumed that the three resistances (or heat flows) are independent so that the dimensionless resistances can be summed in parallel as

$$1/R_j^* = 1/R_c^* + 1/R_g^* + 1/R_r^* \qquad (62)$$

to give the dimensionless joint resistance.

4.1. Experimental Verification of Elastoconstriction and Elastogap Models

Experimental data have been obtained for the elastoconstriction resistance of point contacts [15] and line contacts [12] for a range of sphere and cylinder diameters, material properties and mechanical loads. Data have also been obtained for the verification of the elastogap model for the point [15] and line contacts [12]. The elastogap models have been tested against air, argon, and helium at gas pressures between 10^{-6} Torr and atmospheric.

Some representative test data for the elastoconstriction and elastogap resistances compared with the theoretical values are given in the following sections.

4.1.1. Sphere-Flat Test Results

Kitscha [14] performed experiments on steady heat conduction through 25.4 and 50.8 mm sphere-flat contacts in an air and argon environment at pressures between 10^{-5} Torr and atmospheric. He obtained vacuum data for the 25.4 mm diameter smooth sphere in contact with a polished flat having a surface roughness of approximately 0.13 μm rms. The mechanical load varied from 16 to 46 Newtons. The mean contact temperature ranged between 321 and 316 K. The harmonic mean thermal conductivity of the sphere-flat contact was found to be 51.5 W/mK. The emissivities of the sphere and flat were estimated to be $\varepsilon_1 = 0.2$ and $\varepsilon_2 = 0.8$ thus giving the dimensionless radiative resistance:

$$R_r^* = 3.82\times10^{10}/T_m^3 \qquad (63)$$

The dimensionless constriction resistance is $R_c^* = L$, therefore the dimensionless joint resistance is

$$1/R_j^* = 1/L + 1/R_r^* \qquad (64)$$

The model predictions and the experimental results are compared in Table 2.

It can be seen that the radiative resistance was not negligible; it was approximately 10 times the constriction resistance at the lightest load and 30 times at the highest load. The largest difference between the theory and experiments occurs at the second lightest load where it is approximately -4.7%, within the probable experimental error. These and other vacuum tests [14] have verified the accuracy of the elastoconstriction and the radiation models.

The elastogap model for a point contact was verified by Kitscha [14] and Ogniewicz [18]. For air the gas parameter of Eq. (52) depends upon T_m, P_g and D as follows:

Table 2 Dimensionless load, constriction, radiative and joint resistances of Kitscha [14]

N (Newtons)	L (D/2a)	T_m (K)	R_r^* Eq. (63)	R_j^* Eq. (64)	R_j^* (Test)
16.0	115.1	321	1155	104.7	107.0
22.2	103.2	321	1155	94.7	99.4
55.6	76.0	321	1155	71.3	70.9
87.2	65.4	320	1164	61.9	61.9
195.7	50.0	319	1177	48.0	48.8
266.9	45.1	318	1188	43.4	42.6
467.0	37.4	316	1211	36.4	35.4

$$M = \frac{1.373\times10^{-4}}{D} \cdot \frac{T_m}{P_g} \qquad (65)$$

where D is in cm, T_m in K and P_g in mm H_g. The numerical value of Eq. (65) is based upon air properties at $T_{g,\infty} = 288$ K and $P_{g,\infty} = 760$ mm H_g.

The elastogap model and the experimental results are compared over a range of gas pressures in Table 3. Although tests were conducted at smaller values of the dimensionless parameter L over a range of gas pressures, sphere diameters and gases, the results given in Table 3 are representative of the other data and they also correspond to the case which challenges the validity of the proposed elastoconstriction and elastogap models. First note that the radiative resistance is approximately 10 times the constriction resistance. Second, observe that the gap resistance is approximately 2/3 of the constriction resistance at the highest gas presure, approximately equal to the constriction resistance at a gas pressure between 4 and 40 mm H , and finally 3 times the constriction resistance at $P_g = 0.2$ mm H_g. The agreement between the theory and the tests is very good to excellent.

Table 3 Elastogap Resistance Predictions and Measurements [14] for D = 25.4 mm and Air at L = 115.1

T_m (K)	P_g (mm H_g)	R_g^* Eq. (53)	R_r^* Eq. (61)	R_j^* (Theory)	R_j^* (Test)
309	400.0	76.9	1293	44.5	46.8
310	100.0	87.4	1280	47.8	49.6
311	40.0	97.1	1268	50.6	52.3
316	4.4	137.2	1209	59.5	59.0
318	1.8	167.2	1186	64.5	65.7
321	0.6	227.9	1153	71.7	73.1
322	0.5	246.6	1143	73.4	74.3
325	0.2	345.4	1111	80.1	80.3
321	vacuum	∞	1155	104.7	107.0

The largest difference occurs at the highest gas pressures where the theory predicts lower joint resistances by approximately 5%. The agreement between theory and experiment improves with decreasing gas pressure.

It can also be seen in Table 3, that the air within the sphere-flat gap significantly decreases the joint resistance when compared with the vacuum result.

4.1.2 Cylinder-Flat Test Results

McGee [11] obtained vacuum test data for Zircaloy-4, Keewatin tool steel and Type 304 stainless steel cylinders of diameters 25.4 and 20 mm of lengths 25.4 and 40 mm. The stainless steel cylinder was 20 mm by 40 mm long. The vacuum tests were conducted at 10^{-6} Torr and the total mechanical load was between 80 N and 8000 N.

At light loads ($N^* < 5\times10^{-6}$), agreement between the line contact model and the test results was poor. The higher resistances measured at light loads are due to errors of form (crowning). The actual contact area was elliptical rather than the ideal rectangular contact. This contact area gives a much greater constriction resistance.

As the load increased, the error-of-form effects became negligible because the elliptical contact area grew into a long rectangular contact. For $N^* \geq 5\times10^{-6}$, the measured resistances were observed to be in good agreement with the line contact model predictions. The good agreement was noted for all metals up to the maximum $N^* = 10^{-4}$.

The dependence of joint line contact resistance with fluid pressure was investigated for both helium and argon gas, using the stainless-steel cylinder-flat. Fluid pressure was varied from vacuum where $M = 10^5 - 10^6$ to atmospheric pressure where $M = 10^{-3}$, while a constant load of 2700 N ($N^* = 1.8\times10^{-5}$) was maintained across the contact. The dimensionless joint resistance decreased from 2.5 to 1.5 as the helium pressure increased from vacuum to atmospheric. Very little change in joint resistance occurred until the fluid parameter M approached 1, corresponding to a pressure of 10^{-3} Torr. The resistance decreased significantly between $M = 1$ and $M = 10^{-2}$ then levelled out below $M = 10^{-2}$ as the helium pressure approached atmospheric. The agreement between the line contact gap model and the test results is very good provided $M > 10^{-2}$. The model significantly underpredicts the joint resistance when $M < 10^{-2}$, corresponding to gas pressures approaching atmospheric.

Similar tests were conducted in argon which has a lower thermal conductivity than helium. The test results indicate that the joint resistance is a weak function of gas pressure variations over the observed range of the fluid parameter M. This result is also predicted by the line contact gap model, for fluids having low thermal conductivity, since a large fraction of the heat is conducted through the solid-solid contact area. The theoretical and experimental joint resistances are in good agreement at lower gas pressures ($10^{-2} \leq M \leq 1$). Near one atmosphere, the difference is again significant.

5.1. CONFORMING ROUGH SURFACE MODELS

The problem of predicting and measuring contact, gap, and joint thermal conductances has received considerable attention during the past two decades because of the importance of the topic in many heat-transfer systems. Comprehensive surveys of literature on this subject can be found in several references. Significant progress has been made in our understanding and ability to predict thermal contact conductance. The study of thermal contact conductance in a vacuum is fundamental to our understanding of thermal gap conductance when interstitial fluids are present. The present state of knowledge has reached a point where simple, explicit correlations can be developed for the contact, gap, and joint conductances.

The purpose of this section is to establish correlations for conforming rough surfaces when interstitial fluids such as gases are present in the gap. The proposed correlations will be compared with recently obtained empirical data to demonstrate the validity of the assumptions used to develop the models.

5.1.1. Contact Conductance Correlation

The total constriction resistance of the ith contact spot is

$$R_{ci} = \psi_{ci1}/4k_1a_i + \psi_{ci2}/4k_2a_i \qquad (66)$$

where ψ_{ci1} and ψ_{ci2} are the thermal constriction (or spreading) parameters which depend upon the relative size of the contact spot. Because of geometric and thermal symmetry about the contact plane we can put

$$\psi_{ci1} = \psi_{ci2} = \psi_{ci} = [1 - (a_i/b_i)]^{1.5} \qquad (67)$$

provided $0 < a_i/b_i \leq 0.3$.

If we let $k_s = 2k_1k_2/(k_1 + k_2)$, the harmonic mean thermal conductivity, then Eq. (66) can be written as

$$R_{ci} = \psi_{ci}/2k_sa_i \qquad (68)$$

The total contact resistance of N contact spots thermally connected in parallel is therefore,

$$\frac{1}{R_c} = \sum_{i=1}^{N} \frac{1}{R_{ci}} = 2k_s \sum_{i=1}^{N} \frac{a_i}{\psi_{ci}} \qquad (69)$$

The contact conductance can be derived by means of the following definition:

$$Q_c = h_cA_a\,\Delta T_c = \Delta T_c/R_c. \qquad (70)$$

Therefore,

$$h_c = \frac{2k_s}{A_a} \sum_{i=1}^{N} \frac{a_i}{\psi_{ci}} \qquad (71)$$

Noting that $a_i/b_i \leq 0.3$ and $0.85 \leq \psi_{ci} < 1$, the specific constriction parameter ψ_{ci} appropriate to each contact spot can be replaced by the mean value of the constriction parameter ψ_c based upon the total set of contact spots.

Therefore, we have

$$\psi_{ci} = \psi_c = (1 - \varepsilon)^{1.5} \qquad (72)$$

where $a/b = \varepsilon = \sqrt{A_r/A_a}$. The mean value of the constriction parameter depends upon a and b, the contact spot and associated flux tube radii, respectively, determined by the total real and apparent areas.

A detailed geometric analysis of interacting conforming, rough surfaces yields the following important geometric results:

1) Contact conductance parameter

$$\sum_{i=1}^{N} \frac{a_i}{A_a} = \frac{1}{4\sqrt{(2\pi)}}\,(m/\sigma)\,\exp(-x^2) \qquad (73)$$

2) Relative real contact area

$$\varepsilon^2 = A_r/A_a = \frac{1}{2}\,\mathrm{erfc}(x) \qquad (74)$$

3) Contact spot density

$$n = \frac{1}{16}(m/\sigma)^2 \frac{\exp(-2x^2)}{\text{erfc}(x)} \quad (75)$$

4) Mean contact spot radius

$$a = \sqrt{(8/\pi)}(\sigma/m)\exp(x^2)\,\text{erfc}(x) \quad (76)$$

where $x = Y/\sqrt{2}\sigma$ and Y/σ is called the relative mean plane separation. The surface parameters σ and m are the effective rms surface roughness and the effective absolute surface slope, respectively. They are determined as follows:

$$\sigma = (\sigma_1^2 + \sigma_2^2)^{1/2} \quad (77)$$

and

$$m = (m_1^2 + m_2^2)^{1/2} \quad (78)$$

Assuming plastic deformation of the contacting asperities during the first loading cycle leads to a relationship between the relative real contact area and the relative contact pressure. A force balance on the real and apparent contact areas gives

$$P/H = A_r/A_a = \varepsilon^2 = (1/2)\text{erfc}(x) \quad (79)$$

This relationship between ε and x allows one to compute the other surface parameters. After substitution of the contact conductance parameter, Eq. (73), into the contact conductance expression, Eq. (71), we obtain after multiplying by σ/mk_s the nondimensional contact conductance,

$$(\sigma/m)(h_c/k_s) = \frac{1}{2\sqrt{(2\pi)}} \frac{\exp(-x^2)}{(1-\varepsilon)^{1.5}} \quad (80)$$

with $x = \text{erfc}^{-1}(2P/H)$ and $\varepsilon = \sqrt{P/H}$. The complex expression of Eq. (80) was correlated by the following simple expression:

$$(\sigma/m)(h_c/k_s) = 1.25\,(P/H)^{0.95} \quad (81)$$

which agrees with the exact expression to within $\pm 1.5\%$ for $2 \le Y/\sigma \le 4.75$.

5.1.2. Alternate Development of Contact Conductance

Here we assume N microcontact spots all having the same mean radius a and associated circular flux tube of mean radius b. The total contact resistance is as above

$$R_c = \psi_c/2Nk_s a \quad (82)$$

and the contact conductance is

$$h_c = 2nak_s/\psi_c \quad (83)$$

where n is the contact spot density.

The product of Eqs. (75) and (76) yields

$$na = \frac{1}{4\sqrt{(2\pi)}}(m/\sigma)\exp(-x^2) \quad (84)$$

Substitution of Eq. (84) into Eq. (83) gives Eq. (80). To simplify further calculations, two additional correlations for Y/σ and a are derived.

From Eq. (79) we obtain

$$\sqrt{2}x = Y/\sigma = 1.184[-\ln(3.132P/H)]^{0.547} \quad (85)$$

Multiplying Eq. (76) through by x gives

$$(m/\sigma)ax = \sqrt{(8/\pi)}x\exp(x^2)\text{erfc}(x) \quad (86)$$

In the range of interest $1.41 \le x \le 3.16$, we can write [8]

$$x\exp(x^2)\text{erfc}(x) = 0.52 \quad (87)$$

Substitution of Eqs. (85) and (86) into Eq. (87) yields

$$ma/\sigma = 0.99[-\ln(3.132P/H)]^{-0.547} \quad (88)$$

Knowing the surface characteristics m and σ as well as the relative contact pressure P/H, one can compute the mean contact spot radius by means of Eq. (88).

6.1. Gap Conductance Integral

Heat transfer across the gap formed by the contact of conforming rough surfaces is difficult to analyze because of the complexity of the local geometry which determines whether the local heat transfer can be modelled as continuum, slip or rarefied. To overcome these difficulties it is necessary to model the gap conductance from an overall point of view. To this end it is assumed that the local gap conductance can be modelled as heat conduction between two isothermal parallel plates which are separated by an effective thickness

$$t + M \quad (89)$$

where t is the local gap thickness and $M = \alpha\beta\Lambda$. The gas parameters α, β and Λ are defined by Eqs. (44), (45) and (46) respectively. The modelling of the conforming rough surface gap is similar to that of the elastogap model.

The total gap heat flow rate, Q_g, and the overall gap conductance, h_g, are determined by integration over the effective gap area, A_g,

$$Q_g = \iint_{A_g} \frac{k_{g,=}\Delta T_g\, dA_g}{t + M} = \iint_{A_g} h_g(x,y)\Delta T_g\, dA_g \quad (90)$$

Assuming that the variation of ΔT_g is localized around each contact spot, and therefore $\Delta T_g = \Delta T_c$ over the major portion of the gap, we have

$$h_g = \frac{1}{A_g}\iint_{A_g} \frac{k_{g,=}\, dA_g}{t + M} \quad (91)$$

where

$$h_g = \frac{1}{A_g}\iint_{A_g} h_g(x,y)dA_g \quad (92)$$

is the mean value of the gap conductance over the effective gap area which is given by

$$A_g = A_a(1 - \varepsilon^2) \approx A_a \quad (93)$$

because $\varepsilon < 0.3$.

For gaps formed by two conforming rough surfaces having Gaussian height distributions, an expression for the fraction of the projected gap area, dA_g, is given by

$$dA_g = (A_a/\sqrt{2\pi})\exp[-(Y/\sigma - t/\sigma)^2/2]d(t/\sigma) \quad (94)$$

where t is the local gap thickness and σ is the effective rms surface roughness.

Combining Eq. (93) and (94) leads to the gap conductance and its integral:

$$h_g = (k_{g,=}/\sigma)I_g \quad (95)$$

where

$$I_g = \{1/\sqrt{(2\pi)}\} \int_0^\infty \frac{\exp[-(Y/\sigma - t/\sigma)^2/2]}{(t/\sigma + M/\sigma)} d(t/\sigma) \quad (96)$$

For computational purposes the gap conductance integral can be transformed to

$$I_g = \sqrt{(2/\pi)} \int_0^\infty \frac{\exp[-(n - u^2)^2/2]}{(u^2 + M/\sigma)} u\,du \quad (97)$$

by setting $u^2 = t/\sigma$. The upper limit can be put to a value of 3 for numerical computational purposes because the area under the curve becomes negligible for $u > 2.5$. Hegazy [21] has shown that the approximation of Yovanovich [20]

$$I_g(Y) = [Y/\sigma + M/\sigma]^{-1} \quad (98)$$

is accurate provided the gap parameter $YH = (Y/\sigma)/(M/\sigma) < 1$ for all values of M/σ. The difference between Eqs. (97) and (98) increases for values of $YH > 1$ and $M/\sigma \to 0.1$.

To minimize the difference between the simple approximation, Eq. (98), and the exact integral, Eq. (97), Negus [23] developed the following more accurate approximation:

$$I_g(N) = \gamma_n/(Y/\sigma + M/\sigma) \quad (99)$$

which is based upon Eq. (98) and the tabulated values [20].
The parameter γ_n in Eq. (99) is defined as

$$\gamma_n = 1.063 + 0.095(4 - Y/\sigma)^{1.68}(-\text{Log}_{10}M)^{0.84} \quad (100)$$

for $2 \leq Y/\sigma \leq 4$ and $0.01 \leq M \leq 1.0$, and

$$\gamma_n = 1 + 0.06/M^{0.8} \quad (101)$$

for $2 \leq Y/\sigma \leq 4$ and $1.0 \leq M < \infty$.

Negus reports the maximum difference between the exact values based upon a numerical quadrature of Eq. (97) and those of the new approximations appears to be about 2% for Y/σ close to 2 and 4.

6.1.1. Dimensionless Joint Conductance Correlation

The contact and gap heat transfer rates are approximately independent for most practical contact problems. If the radiative heat transfer rate across the gap is assumed to be negligible, the total or joint coductance, h_j, for conforming rough surfaces is equal to the sum of the contact and gap conductances developed above. Therefore,

$$h_j = h_c + h_g \quad (102)$$

Multiplying by $(\sigma/m)k_s$ to non-dimensionalize gives

$$(\sigma/m)(h_j/k_s) = (\sigma/m)(h_c/k_s) + (\sigma/m)(h_g/k_s) \quad (103)$$

or for convenience

$$C_j = C_c + C_g \quad (104)$$

7.1. Experimental Verification of Contact, Gap and Joint Conductances

Experimental data have been recently obtained by Hegazy [21] which provide ample evidence that the conforming, rough surface contact and gap conductance models are very accurate. Data were obtained under vacuum conditions, $P < 10^{-5}$ Torr, for Nickel 200, type 304 stainless steel, Zircaloy-4 and Zr-2.5 wt% Nb alloys. Each interface consisted of a relatively smooth, lapped surface and a rough, bead-blasted surface of identical material. The surface parameter (σ/m) was 8.20 μm to 12.4 μm for the smoothest interfaces and it was 38.3 μm to 59.8 μm for the very rough interfaces. The mean interface temperature, T_m, ranged from 372K to 451K. The bulk hardness of the metals, H_b, ranged from 1010 MPa to 1727 MPa and the contact hardness, H_c, was determined to be 1972 MPa for the very rough Zirconium-4 interface at the highest load and 4113 MPa for the smooth SS304 interface at the lightest load.

The contact hardness, H_c, was determined by means of a mechanical model recently developed by Yovanovich and co-workers [21] for bead-blasted surfaces. The model is based upon a least squares fit of Vickers microhardness measurements obtained at several loads, and a geometric-mechanical model which is based upon a force balance applied to a contact formed by a typical asperity produced by bead-blasting. Hegazy [21] reports that the effective contact hardness can be determined by means of the following expression based upon a relative contact pressure of $P/H = 10^{-3}$:

$$H_c = c_1(0.95\sigma/m)^{c2} \quad (105)$$

where c_1 and c_2 are Vickers microhardness correlation coefficients,

$$H_v = c_1 d_v^{c2} \quad (106)$$

and d_v is the measured Vickers diagonal. The microhardness values are GPa and the Vickers diagonal is in μm. The correlation coefficients are given in Table 4.

Table 4 Hegazy Vickers Microhardness Correlations, $H_v = c_1 d_v^{c2}$

Material	H_m, GPa	c_1	c_2	Max % Diff.	RMS % Diff.
Zr-4	1.913	5.677	-0.278	3.4	1.7
Zr-2.5wt%Nb	1.727	5.884	-0.267	10.2	2.7
Ni200	1.668	6.304	-0.264	4.8	1.8
SS304	1.472	6.271	-0.229	4.2	1.4

Hegazy also developed the following approximate, semi-general microhardness correlation of the metals given in Table 4:

$$H_c = (12.2 - 3.54\,H_b)(\sigma/m)^{-0.26} \quad (107)$$

where H_c, the contact hardness, and H_b, the bulk hardness are in GPa, and the effective surface parameter (σ/m) is in μm. This relationship shows clearly how H_c depends upon H_b and the surface roughness.

Thermal contact conductance values were measured for five different interfaces for the metals listed in Table 4. For apparent contact pressures ranging between approximately 0.45 MPa to 8.90 MPa the measured contact conductance for all metals is in very good to excellent agreement with the new model predictions. Typical results are presented in Figure 1 for two stainless steel interfaces, the smoothest and the roughest. The solid lines are the theoretical values based upon the appropriate values of the contact microhardness which Hegazy [21] reports are approximately 4100 MPa and 2510 MPa respectively, and the measured bulk hardness

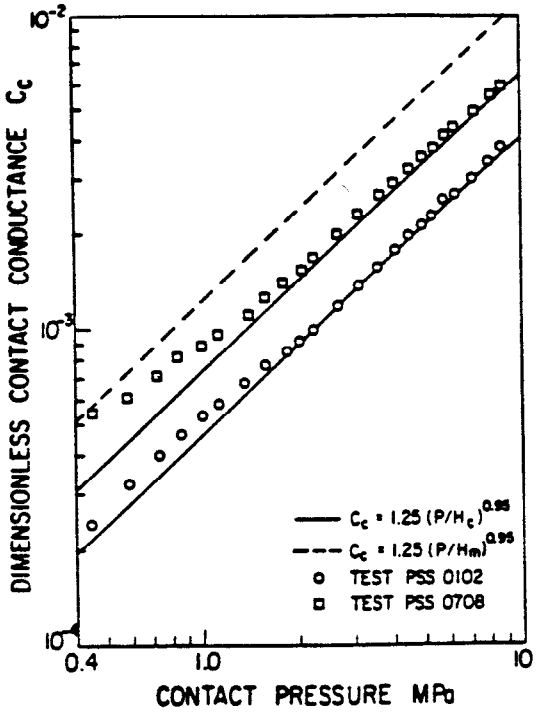

Figure 1 Comparison of theoretical and measured contact conductances for type 304 stainless steel [21]

was 1470 MPa. The dashed line represents the model predictions based upon the bulk hardness. The differences observed at light contact pressures P < 2 MPa is attributed to several factors which are not accounted for in the present model. One of the major factors may be thermal strains induced at the microcontacts due to very large temperature drops and local temperature gradients.

The gap and joint conductance models were also verified by Hegazy [21] who measured contact and joint conductances for a stainless steel interface with nitrogen gas at a gas pressure of approximately 40 Torr. The surface parameter σ/m = 32.3 μm, the gap parameter YH was approximately 2.4. The dimensionless conductances are plotted versus the dimensionless contact pressure in Figure 2 where it can be seen that the vacuum results are in excellent agreement over the full load range and the joint conductances are in very good agreement over a limited range of the contact pressure.

To verify the joint conductance model at a higher gas pressure, Hegazy measured joint conductances only for nitrogen gas at a pressure of approximately 570 Torr between stainless steel surfaces having σ/m = 36.9 μm. The gap parameter YH was approximately 29 to 38 over the entire load range. The measured results are compared with the model results in Figure 3.

The measured values are above the predictions over the entire load range. The model clearly predicts the effect of increasing load, but underpredicts the joint conductance by approximately 10 to 15%.

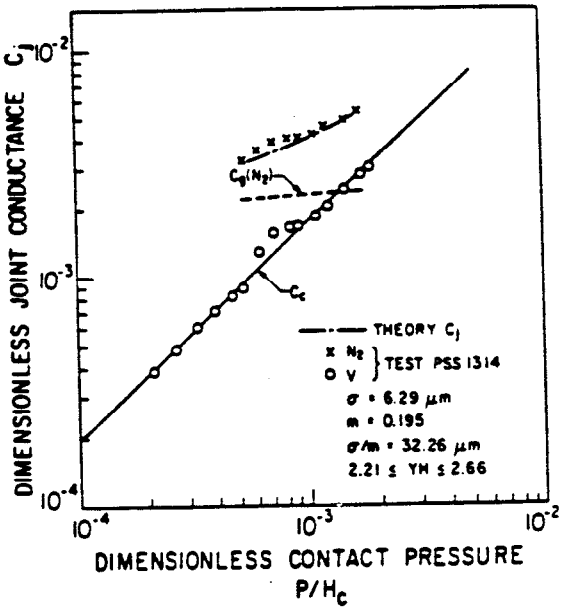

Figure 2 Comparison of theoretical and measured joint conductances for type 304 stainless steel and nitrogen gas [21]

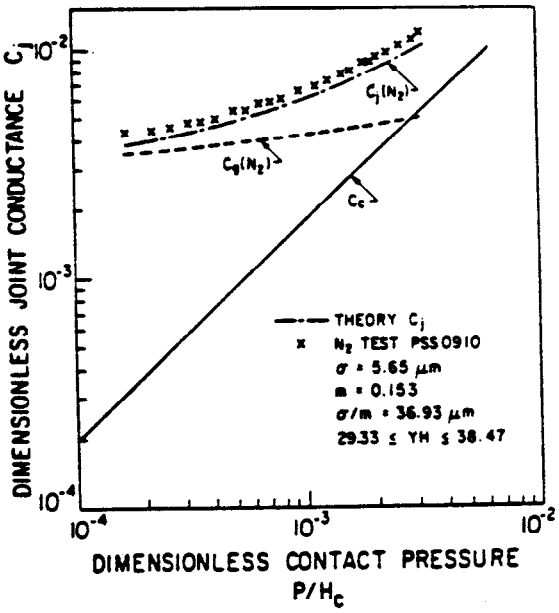

Figure 3 Comparison of theoretical and measured joint conductances for type 304 stainless steel and nitrogen gas [21]

7. ACKNOWLEDGEMENTS

The continued support of the Canadian Natural Science and Engineering Research Council has made this work possible. The author acknowledges the many graduate research assistants who helped make the research successful.

8. REFERENCES

1. Yovanovich, M.M., Thermal Constriction Resistance between Contacting Metallic Paraboloids: Application to Instrument Bearings, Progress in Aeronautics and Astronautics, Heat Transfer and Spacecraft Thermal Control, Vol. 24, editor, Dr. J.W. Lucas, MIT Press 1971, pp. 337-358.
2. Yovanovich, M.M., Thermal Contact Resistance across Elastically Deformed Spheres, J. Spacecraft Rockets, Vol. 4, p. 119, 1967.
3. Yovanovich, M.M., Simplified Explicit Elastoconstriction Resistance Expression for Ball/Race Contacts, AIAA 78-84, AIAA Aerospace Sciences Meeting, 1978.
4. Timoshenko, S.P. and Goodier, J.N., Theory of Elasticity, McGraw-Hill Book Company, 3rd edition, New York, 1970, Chap. 12.
5. Kornhauser, M., A Note on Elastic Surface Deformation, J. of Appl. Mech., Vol. 18, pp. 251-252, 1951.
6. Cooper, D.H., Hertzian Contact-Stress Deformation Coefficients, J. of Appl. Mech., Vol. 36, pp. 296-303, 1969.
7. Walowit, J.A. and Anno, J.N. Modern Developments in Lubrication Mechanics (Applied Science Publishers, Barking, Essex, 1975.
8. Abramowitz, M. and Stegun, I., Handbook of Mathematical Functions, Dover Publication, 1965.
9. Yovanovich, M.M. and Coutanceau, J., Sur al dètermination de la resistance thermique tranversale d'un cylindre de revolution homgène isotrope avec des conditions aux limites mixtes, C.R. Acad. Sci. Paris 268 (1969) B821-B823.
10. Veziroglu, T.N. and Chandra, S. Thermal Conductance of Two-Dimensional Constrictions, in: Thermal Design Principles of Spacecraft and Entry Bodies, Prog. Astronautics and Aeronautics, Vol. 21, ed. J.T. Bevans AIAA, New York, pp. 591-651, 1969.
11. McGee, G.R., An Analytical and Experimental Study of the Heat Transfer Characteristics of Cylinder-Flat Contacts, M.A.Sc. thesis, University of Waterloo, 1982.
12. McGee, G.R., Schankula, M.H., and Yovanovich, M.M., Thermal Resistance of Cylinder-Flat Contacts: Theoretical Analysis and Experimental Verification of a Line-Contact Model, Nuclear Engineering and Design, Vol. 86, pp. 369-381, 1985
13. Kaganer, M.G., Thermal Insulation in Cryogenic Engineering, translated from Russian by A. Moscona (Israel Program for Scientific Translations, Jerusalem, 1969).
14. Kitscha, W.W., Thermal Resistance of Sphere-Flat Contacts, M.A.Sc. thesis, Dept. of Mechanical Engineering, University of Waterloo, 1982.
15. Kitscha, W.W., and M.M. Yovanovich, Experimental Investigation on the Overall Thermal Resistance of Sphere-Flat Contacts, Heat Transfer with Thermal Control Applications, M.M. Yovanovich, ed., Vol. 39 of Progress in Astronautics and Aeronautics, AIAA, MIT Press, Cambridge, MA, 1975.
16. Yovanovich, M.M., and W.W. Kitscha, Modelling the Effect of Air and Oil upon the Thermal Resistance of a Sphere-Flat Contact, Thermophysics and Spacecraft Thermal Control, R.G. Hering, ed., Vol. 35 of Progress in Astronautics and Aeronautics, AIAA, MIT Press, Cambridge, MA, 1974.
17. Burde, S.S. and M.M. Yovanovich, Thermal Resistance at Smooth Sphere/Rough Flat Contacts: Theoretical Analysis, Thermophysics and Thermocontrol, R. Viskanta, ed., Vol. 65 of Progress in Astronautics and Aeronautics, AIAA, New York, 1979.
18. Ogniewicz, Y., Conduction in Basic Cells of Packed Beds, M.A.Sc. thesis, Dept. of Mechanical Engineering, University of Waterloo, 1975.
19. Ogniewicz, Y., and M.M. Yovanovich, Effective Conductivity of Regularly Packed Spheres: Basic Cell Model with Constriction, Heat Transfer and Thermal Control Systems, L.S. Fletcher, ed., Vol. 60 of Progress in Astronautics and Aeronautics, AIAA, New York, 1978.
20. Yovanovich, M.M., J. DeVaal, and A.H. Hegazy, A Statistical Model to Predict Thermal Gap Conductance Between Conforming Rough Surfaces, AIAA Paper 82-0888, presented at the AIAA/ASME Third Joint Thermophysics, Fluids, Plasma and Heat Transfer Conference, 1982.
21. Hegazy, A.A., Thermal Joint Conductance of Conforming Rough Surfaces: Effect of Surface Micro-Hardness Variation, Ph.D. thesis, University of Waterloo, 1985.
22. Blahey, A., Personal Communication, University of Waterloo, 1981.
23. Negus, K.J., Personal Communication, University of Waterloo, 1985.